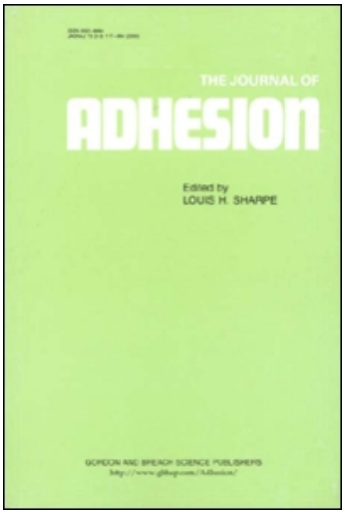

The Journal of Adhesion

Publication details, including instructions for authors and subscription information:
http://www.informaworld.com/smpp/title~content=t713453635

Peel Adhesion: Rate Dependence of Micro Fracture Processes

D. H. Kaelble[a]; R. S. Reylek[a]
[a] Central Research Laboratories, 3M Co., St. Paul, Minn.

To cite this Article Kaelble, D. H. and Reylek, R. S.(1969) 'Peel Adhesion: Rate Dependence of Micro Fracture Processes', The Journal of Adhesion, 1: 2, 124 — 135
To link to this Article: DOI: 10.1080/00218466908078883
URL: http://dx.doi.org/10.1080/00218466908078883

Peel Adhesion: Rate Dependence of Micro Fracture Processes

D. H. KAELBLE AND R. S. REYLEK

Central Research Laboratories, 3M Co.
St. Paul, Minn. 55119

(Received February 21, 1969)

ABSTRACT

The micro-fracture mechanism of peeling is studied by means of a "bond stress analyses" which permits direct measurement of the distribution of normal or "cleavage" type stresses localized at the propagating boundary of failure. Improved instrumentation now permits direct stress analysis over nearly three decades of peeling rate. Experimental stress distributions are presented for an acrylic adhesive peeled from stainless steel. This study covers the transition region from elastomeric to flow state response where the viscoelastic transition from apparent interfacial to cohesive failure is observed for this acrylic copolymer. The major features of the cleavage stress distribution are qualitatively interpreted in terms of a cavitation-filamentation model which describes entanglement slippage as the dominant rate factor for cleavage response.

INTRODUCTION

A PREVIOUS paper has discussed a new instrument called a "bond stress analyzer" which permits direct measurement of the distribution of normal stresses in an adhesive bond during peel [1]. Analysis of the detailed form of the normal stress distribution identifies a complicated process of micro cavitation and adhesive orientation which contributes importantly to the bond strength. These same micro-fracture processes may also figure prominently in determining whether final unbonding is interfacial or cohesive in nature. In viscoelastic adhesives it is well known that peeling force is very rate dependent and that transitions from adhesive to cohesive failure can occur from peel rate changes [2].

This discussion describes the influence of peel rate on the micro cavitation and orientation processes in an elastomeric adhesive interlayer bonded to stainless steel. The study was accomplished by use of an improved version of the original bond stress analyzer. The new instrument is provided with an extended frequency range of response which permits stress analysis to be conducted over nearly three decades of peel rate. Improved sensitivity also provides much better definition of the fine structure of the stress distribution curves.

INSTRUMENTATION

The previously described instrument was restricted by the character of the weighing system design, external to the force transducer, to bond stress wave frequencies less than $V = 0.10$ cycles/sec. where the frequency is related to stress wave length λ, peel rate r, and the bond stress concentration factor β by the following relation [2]:

$$V = r/\lambda = \frac{\beta r}{2\pi} \tag{1}$$

The stress concentration factor is defined by peel adhesion theory by the following equation:

$$\beta = \left[\frac{9\ G(t)}{8\ E\ h^3\ a} \right]^{1/4} \tag{2}$$

where:

E = Young's modulus of the flexible member, in this case, the pressure sensitive tape backing.
h = half thickness of the flexible member.
$G(\omega)$ = shear modulus of the viscoelastic adhesive at frequency ω.
a = thickness of adhesive layer.

The parameters of equation (2) describe the stress concentration factor in terms of bond rheology and geometry. Knowing these properties and peel rate the stress wave frequency V may be calculated.

The previously described instrument was designed to operate as an integrally mounted Instron accessory. The redesigned unit is mechanically and electronically independent of the Instron Tensile Tester. The only function of the Instron in the modified design is to control the bonding and peel rates.

The circuit diagram of Figure 1 describes the weighing system of the new instrument. The original configuration of a 50 kg Instron CM load cell in the bond stress analyzer assembly was maintained. As indicated in Figure 1, the load cell power supply, signal modulation, and recording components operate independently of the Instron and provide an upper frequency limit of $V = 8.0$ c/s for both the direct and differentiated signal. This upper limit was imposed by the necessity to introduce a low pass filter with a sharp cut off frequency at 85 c/s in order to prevent damage to the Visicorder galvanometers. Improved differentiator response was obtained by introducing a Dymec high gain negative-feedback amplifier as shown in Figure 1.

The basic wave form of the peel stress signal is sinusoid with a circular frequency $\omega = 2\pi V$. Superimposed upon this basic wave form are higher frequency components to be later discussed as secondary components. Electrical differentiation tends to accentuate irregularities in the signal being

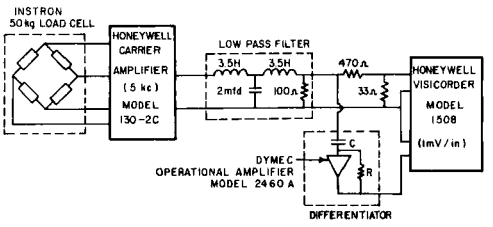

Figure 1. Force measuring system of the bond stress analyzer.

differentiated. These irregularities are due to electrical noise developed internally in the circuit (principally 60 c/s line noise and 5000 c/s from unfiltered frequency noise) and external mechanical vibration which generates a noise signal in the load cell (primarily from Instron motors and generally above 20 cps). The mechanical noise problem was solved by mounting the bond stress analyzer on a vibration isolating table independent of the Instron frame. The low pass filter satisfactorily eliminated the 5000 cycle electrical noise. Selection of Visicorder galvanometers of the M4035A Heiland type with a natural response frequency of 40 c/s effectively suppressed the 60 c/s line noise.

Considering now the stress wave signal as a true sinusoid the actual output of a simple series resistance-capacitance (R-C) differentiator is [3]:

$$e_o = RC \frac{d}{dt} (e_i - e_o) \tag{3}$$

whose standard solution is:

$$e_o = e_i \frac{RC\omega}{\sqrt{1 + (RC\omega)^2}} \cos(\omega t - \phi) \tag{4}$$

where ϕ is the phase angle, $\tan \phi = RC\omega$, between the true derivative of the input signal, $e_i \sin\omega t$, and the observed derivative given by equation (3). For ideal differentiation, Jeffries [4] concludes that $\tan \phi$ should be less than 0.01. Obviously for ϕ to be small the value of $RC\omega$ should be small. But as indicated in equation (4) this also leads to very small output voltages e_o, which represents the differentiated signal, relative to the input voltage e_i.

By use of an operational amplifier in the configuration shown in Figure 1 the output of the differentiator circuit is [3, 5]:

$$e_o \left(1 + \frac{1}{A}\right) = -RC \frac{d}{dt} [e_i - (e_o/A)] \tag{5}$$

where $(-A)$ is the amplifier gain. Where the amplifier gain factor is high, $(-A) >>> 1.0$ and $(-A) >>> 1 + RC\omega$ equation (5) simplifies to:

$$e_o = -RC \frac{de_i}{dt} = -e_i RC\omega \cos\omega t \tag{6}$$

The unit used in this circuit displays a voltage gain of $(-A) \geqq 10{,}000$ at frequencies below $V = 50$ c/s, and satisfies both assumptions involved in the above simplification. Equation (6), which is the operating equation of the differentiating circuit, indicates that the output voltage e_o can be maintained comparable to input voltage e_i by providing that $RC\omega = 1.0$. For the highest frequencies used $\omega = 2\pi V \simeq 50$ rad/s it follows that $A \simeq 500$ and the second assumption for equation (6), namely $A >> 1 + RC\omega$, is well satisfied.

EXPERIMENTAL

This new apparatus was applied to the further characterization of adhesion phenomena of a self-bonding tape whose bulk and interfacial properties have previously been well characterized [6]. This tape is a construction of a polyester (polyethylene terephthalate) tape backing and an acrylic copolymer adhesive which is free of low molecular weight additives or inorganic fillers. The previous study of the peel adhesion properties of this tape had revealed a critical range of peel rates, roughly from .01 to 10 cm/min. at 23°C., in which peel force maxima were exhibited. These peel force maxima were displayed independent of the failure mechanism, either interfacial adhesive or bulk adhesive failure, and independent of the nature of the substrate.

The tape was bonded to the stainless steel surface of the bond stress analyzer by use of a bonding accessory. The bonding device is critically aligned such that its direction of motion and roller rotation is perpendicular to the line of discontinuity on the test surface of the bond stress analyzer. The tape, of width just equal to the roller width of 1.27 cm, is carefully aligned, adhesive side out, on the bonding wheel. The tape is transferred from the wheel to the stainless steel surface on the first pass of the roller. This special technique of applying the tape to the stress analyzer surface assures its orientation relative to the gap and establishes its positive alignment beneath the bonding roller. A total of six passes using a bonding force of 1000 gm and constant speed of 10 cm/min. are applied to accomplish the bonding process. The resultant bond is free of visible bubbles or defects and produces quite reproducible results in terms of both peel force and internal stress distribution profiles. The time lapse between bonding and peeling which may range from one to five minutes did not influence the results. A stainless steel bonding roller of 4.81 cm. diameter was utilized for these experiments.

In peeling for stress analysis the bonding assembly is retracted just out of contact with the analyzer surface. The lower end of the bonded tape is folded back on itself and its adhesive side adhered to the locked roller surface. The roller assembly through motion of the Instron crosshead then

serves to transmit the desired peel rate condition to the bond at a peel angle of 180 degrees.

Bonds were established in the manner described and peel stress profiles obtained at different rates which range from 25 cm/min to .05 cm/min. Traces of the recorded stress profiles are presented in Figure 2 through Figure 5. At all rates except 0.05 cm/min, two or more stress profiles were measured. These are shown superimposed on the illustrations. The base line for each set of superimposed profiles represents the condition of zero bond stress. Portions of the curves below this line represent the condition of compressive stress and curve sections above the base line tensile stress. The scale of stress and distance are indicated for each set of profiles. These scales differ for the different rates due to changes in the measuring sensitivity and recorder chart speed settings.

The lower section of Figure 5 provides a schematic orientation of a typical stress profile relative to the peel profile of the bond. Identified on this lower figure are four characteristics of the peel stress distribution for which data have been individually tabulated. The characteristic half wave length ($\lambda/2$) is determined from the profile length under compression. These prominent stress values, the maximum compressive stress σ_c, the primary tensile stress maximum σ_{t1}, and the secondary stress maximum σ_{t2}, are also tabulated. The profiles presented in Figure 2 through Figure 5 are tracings from the primary record and are primarily illustrative in form rather than being accurate representations of the direct record. The summary of the experimental results in terms of these four parameters of the stress profile are presented in Table 1.

Table 1. Averaged Characteristics of the Peel Stress Distribution

Rate r cm./min.	Peel Force P (gm.)	No. of Tests	$\lambda/2$ (cm.) Ave.	$\lambda/2$ (cm.) Dev.(±)	σ_c (gm./cm.²) Ave.	σ_c (gm./cm.²) Dev.(±)	σ_{t1} (gm./cm.²) Ave.	σ_{t1} (gm./cm.²) Dev.(±)	σ_{t2} (gm./cm.²) Ave.	σ_{t2} (gm./cm.²) Dev.(±)
25.0	477	3	0.025	.0023	10600	1910	8800	1080	—	—
18.5	—	3	0.025	.0003	9710	730	7640	605	—	—
12.5	418	3	0.029	.0007	7620	237	7000	830	—	—
8.5	—	3	0.028	.0013	8220	1290	8240	860	—	—
5.0	343	3	0.028	.0010	6820	120	7430	180	3910	0
3.5	—	3	0.028	.0003	7470	280	8770	180	2700	205
2.5	298	7	0.028	.0013	7970	690	8830	870	3980	1800
1.85	—	4	0.027	.0012	8130	410	8570	970	6130	510
1.25	264	4	0.030	.0044	6900	415	7410	370	6800	0
0.85	—	5	0.031	.0052	5950	1050	6220	950	4260	660
0.50	210	3	0.031	.0050	5650	940	8870	1850	6150	1180
0.35	—	3	0.028	.0007	5580	217	7050	950	5270	1110
0.25	172	5	0.033	.0047	4740	910	5320	490	3750	1140
0.185	—	3	0.035	.0044	4250	890	5230	2100	2800	240
0.125	128	2	0.031	.0020	3280	2	3260	520	—	—
0.05	32.5	1	0.021	—	3150	—	3450	—	—	—

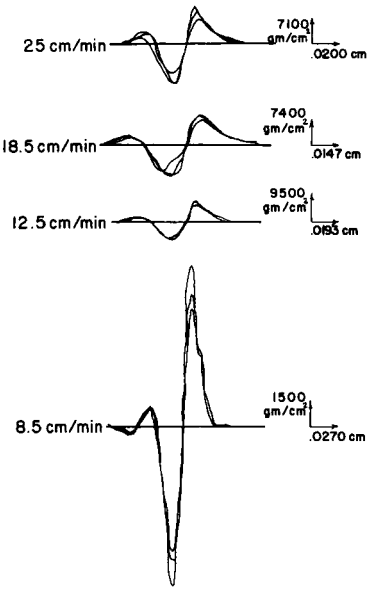

Figure 2. Stress distribution envelopes.

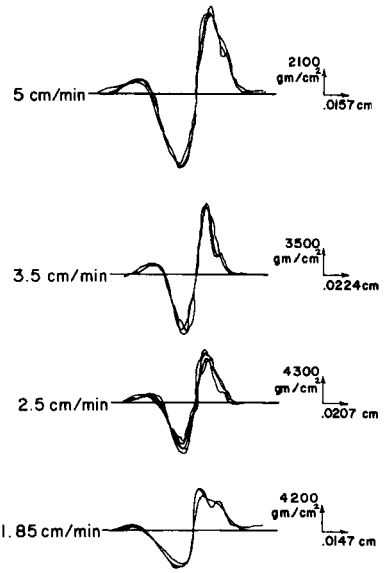

Figure 3. Stress distribution envelopes.

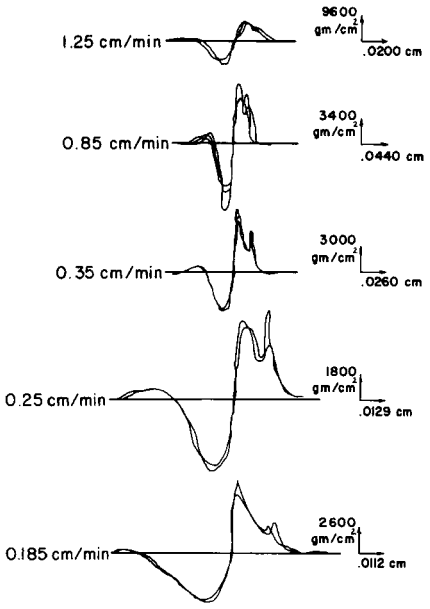

Figure 4. Stress distribution envelopes.

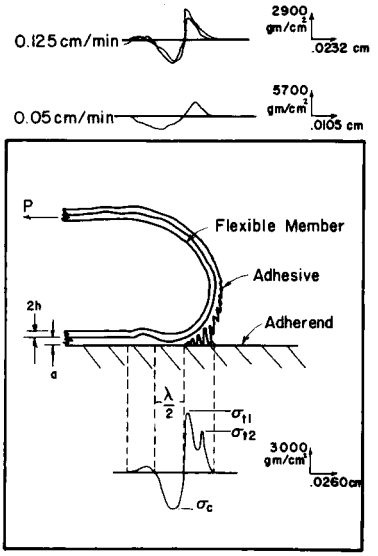

Figure 5. Stress distribution envelopes and schematic representation of the peel profile.

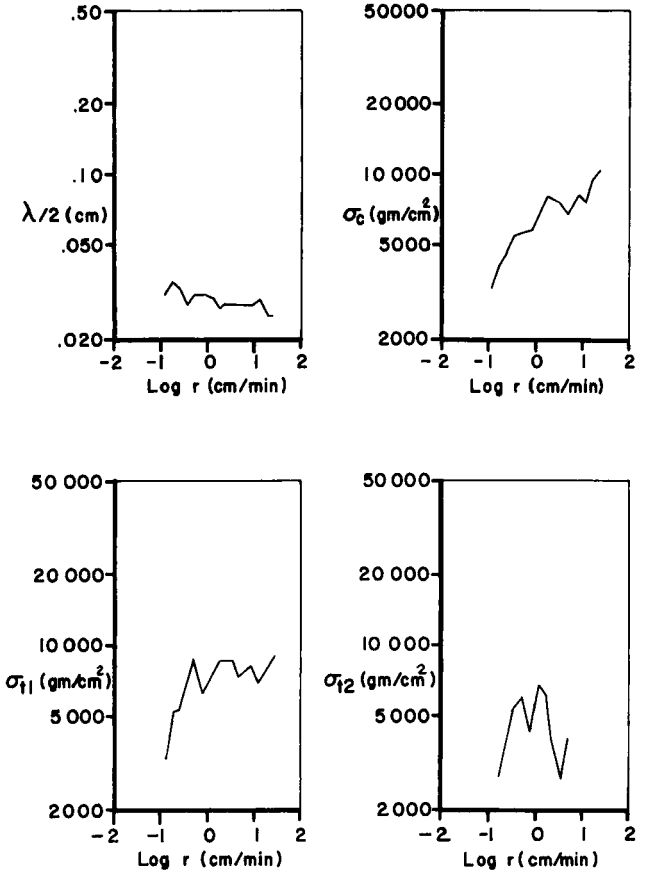

Figure 6. Rate dependence of four characteristic features of the peel stress distribution.

The rate dependence for each of the four prominent characteristics of the peel stress distribution is illustrated on the bilogarithmic graphs of Figure 6. These graphs represent the averaged result for each rate which is tabulated in Table 1. The unsmoothed curves presented in Figure 6 illustrate fairly regular trends in each of the four parameters which will be the subject of analysis in the following section.

DISCUSSION

A previous study [6] of peel adhesion properties has established the rate dependence of peel force described in Figure 7 for the same tape utilized in this experiment. Figure 7 presents the peel force-rate master curves, representative of 23°C. and 180 degree peel, for eight substrate surfaces. The

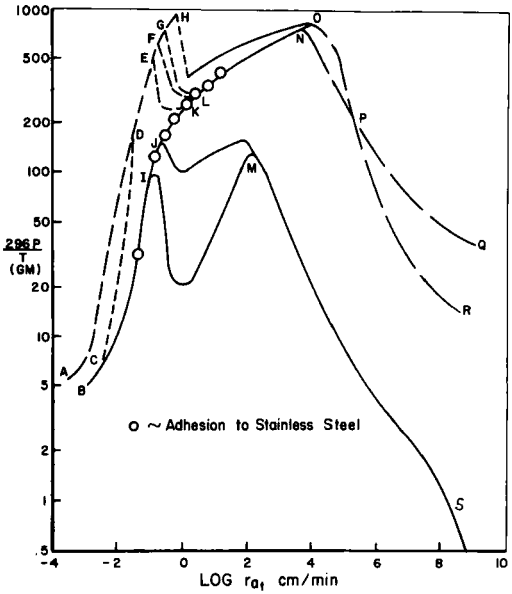

Figure 7. Temperature reduced peel force versus peel rate master curves to eight substrates for a reference temperature of T_o = 296°K = 23°C.

terminal and junction points of the various curve segments of Figure 7 have been letter coded. The peel force vs. rate curve for each substrate studied may be identified by the particular curve which matches the simplest connection of the letter code points described below:

Substrate	Letter Code Points
Glass	ADFLNOPR
Nylon 6	BCKNOPR
Polystyrene	ADEHOPR
Kel-F	BCDGLNOPR
Polyvinylfluoride	ADFLNPQ
Polyvinylidenefluoride	ADGLNPQ
Teflon TFE	BCIMS
Teflon FEP	BCJMS

The curve segments of Figure 7 are further described in terms of four mechanisms of unbonding which are:

Curve Type	Mechanism of Failure
Solid	Interfacial adhesive from adherend
Long dash	Interfacial adhesive from backing
Medium dash	Cohesive within the adhesive
Short dash	Transition between above mechanisms

The peel force versus rate data of this study on stainless steel, see Table 1, follows the Nylon 6 curve of Figure 7. An equivalent mechanism of failure, apparent interfacial unbonding between adhesive and adherend, is also presented for both stainless steel and Nylon 6. The adhesion properties of Nylon 6 and apparently stainless steel are somewhat peculiar in their rate dependence. At rates less than 0.5 cm/min the peel forces are equivalent to a low adhesion surface such as Teflon. Peel rates above 0.5 cm/min. produce peel forces characteristic of a high adhesion surface such as glass. The reasons for this particular type of rate dependence of adhesion properties are not clarified by either interfacial energy or rheological considerations [6].

The rheological properties of the polyacrylic adhesive interlayer are fully described, for low deformations, by the shear relaxation modulus curve presented in Figure 8. These data are represented from a previous report [6] and were obtained by standard experimental techniques described by Tobolsky [7]. The time scales of the peel adhesion experiments and the stress relaxation experiments may be related by equation (1) which is restated here in more appropriate form:

$$\frac{1}{t} = \omega = \frac{2\pi r}{\lambda} \tag{7}$$

where t is relaxation time, ω is the circular frequency, and $\lambda/2$ the half wave length of the cleavage stress wave. Table 1 and Figure 8 indicate that $\lambda/2 = 0.03 \pm .005$ cm. is a nearly constant value over the range of rates studied here. Applying this value ($\lambda/2$) to equation (7) we obtain the appropriate proportionality relation:

$$\frac{1}{t}(\text{sec.}^{-1}) = \left(\frac{\pi}{.03}\,\text{cm.}^{-1}\right)\left(.0167\frac{\text{min.}}{\text{sec.}}\right) r\ \text{cm./min.}$$
$$= 1.75\left(\frac{\text{min.}}{\text{cm. sec.}}\right) r\ \text{cm./min.} \tag{8}$$

which relates the reciprocal time scale of Figure 8 with the peel rate scale of Figure 7. In other words, a peel rate, r, .57 cm/min. corresponds to a relaxation time, t, of 1.0 second by the above relation.

Present peel theory does not treat the complicated stress distribution functions displayed in Figures 2 through Figure 5. In fact, the process of micro cavitation and orientation within the adhesive interlayer has only recently been recognized as an important contribution to the measured peel force [1]. The curves of Figure 6 do indicate that prominent features of the normal stress distribution display more or less regular variations with rate.

As shown in Figure 6, the half wave length of the stress wave ($\lambda/2$) diminishes only slightly with increased rate. This effect follows a prediction

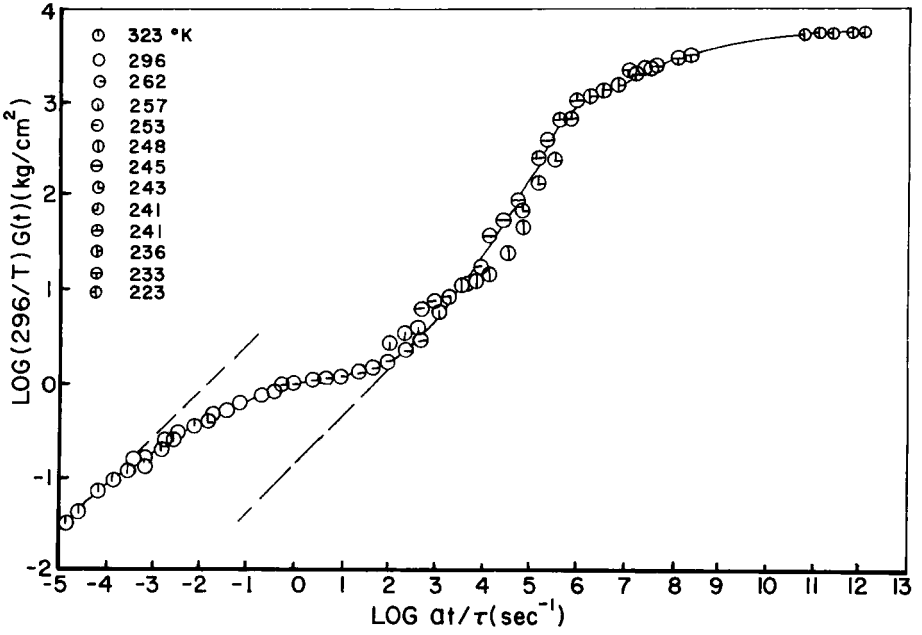

Figure 8. Temperature reduced shear relaxation modulus versus reciprocal time for the tape adhesive at a reference temperature of T_o = 296°K = 23°C.

of theory [8] which involves the following correlation:

$$(\lambda/2) \propto G^{-1/4}$$

where G is the shear modulus of the adhesive interlayer. At higher rates the effective shear modulus is increased causing a decrease in $(\lambda/2)$ by a reciprocal ¼ power change.

The averaged data for maximum compressive stress σ_c, illustrated in Figure 6, displays a dependency on rate which closely parallels the peel force values represented in Figure 7 by curve BCIJL. It is quite obvious from Figure 6 that the rate dependencies of σ_c and the primary peak tensile stress σ_{t1} are not equivalent.

The σ_{t1} peak has been associated in previous discussion [1] with the onset of a cavitation process in the adhesive interlayer. The lower left curve of Figure 6 indicates that σ_{t1} is quite rate dependent below $r = 0.5$ cm/min. At higher rates, up to 25 cm/min, the σ_{t1} values are essentially rate independent while peel force and adhesive shear modulus both increase with rate. This result is in contradiction to predictions of peel theory [8] which ignores the cavitation and orientation processes apparent here. Peel theory, which describes an idealized sharp fracture condition, presents the following proportionality:

$$P \propto \sigma_o^2/G$$

where P is peel force, G is adhesive shear modulus and σ_o is the idealized tensile fracture stress. The above proportionality predicts that σ_o should increase as P and G increase with rate. The fact that σ_{t1} does not follow this prediction directs attention to the secondary tensile stress peak σ_{t2}.

It has been previously argued [1] that the existence of the secondary tensile stress peak σ_{t2} depends upon molecular orientation within the highly elongated strands of adhesive. The rate dependence of σ_{t2} should then yield some information concerning this orientation process. The lower right curve of Figure 6 displays the rate dependence of the average σ_{t2} values. The σ_{t2} values display a notable maxima and become nearly equivalent to σ_{t1} values in the peel rate range from 0.3 to 2.0 cm/min. Figure 7 illustrates the fact that this is the same range of rates at which the adhesive displays a characteristic transition from interfacial to cohesive failure on a number of adherends. The rate to time proportionality of equation (8) and the modulus curve of Figure 8 further illustrates that the transition from rubbery to flow properties in the adhesive roughly coincides with the rate range of the σ_{t2} maximum. We have then established the coincidence of the σ_{t2} maximum, the transition region of the interfacial to cohesive failure mechanisms, and the transition from rubbery to flow regions of viscoelastic response.

This correlation of these three separate phenomena with regard to rate or time scales suggests a very qualitative hypothesis concerning the cavitation-orientation process. At rates below 0.1 cm/min. or reciprocal relaxation times less than .175 sec.$^{-1}$ extensive "entanglement slippage" [1, 6, 7] within the adhesive polymer network permits extensive cavitation but prevents molecular orientation within the elongated strands. At rates above 2.0 cm/min. or reciprocal relaxation times above 3.7 sec.$^{-1}$ the stability of the adhesive entanglement network prevents extensive cavitation growth which is a prerequisite for strand formation and strand orientation. Between these lower and higher peel rates the rate of entanglement slippage comes into coincidence with the rate of adhesive deformation such that both the cavitation and orientation processes are permitted, thus leading to the maximizing of the σ_{t2} values.

The location of the σ_{t2} stress peak, as shown in the schematic of Figure 6, has the effect of redistributing the average forces over a greater length of the bond. General equations which define the mechanics of peel, independent of the particular form of the normal stress distribution [9], point out that this results in an increase in the internal moment of force in the bond and to an increase in peel force.

The transition from interfacial to cohesive failure is only partly explained by this proposed mechanism of the σ_{t2} maxima. It is very likely that cavitation occurs both at the bond interface and in the bulk of the adhesive simultaneously. The competition in these two cavitation processes combined with

the strand orientation mechanism may figure importantly in the correct final explanation of the peel force versus rate curves presented in Figure 8.

SUMMARY AND CONCLUSIONS

The instrument described in this discussion provides a new type of quantitative data for the analysis and understanding of the micromechanisms of fracture which may control polymer adhesion properties. The analysis presented here of rate effects, through the interfacial to cohesive failure transition region, on these micro-fracture mechanisms strongly suggests the need for additions to the theory of peel adhesion which will treat these processes.

A logical extension of this study involves modification of the instrument to permit variable temperature measurement and the application of time-temperature superposition directly to the normal stress distribution curves. This extension would permit detailed examination of the micro-mechanisms of peel over a very broad range of reduced rate such as presented in Figure 8.

REFERENCES

1. D. H. Kaelble, *Trans. Soc. Rheol.*, 9:2, (1965), p. 135.
2. D. H. Kaelble, *J. Coll. Sci., 19,* (1964), p. 413.
3. W. W. Soroka, *Analog Methods of Computation and Simulation,* 82, McGraw-Hill Book Co., New York (1954).
4. R. J. Jeffries, *Instruments, 22,* (1949), p. 1106.
5. S. Fifer, *Analogue Computation,* Vol. 1, 39, McGraw-Hill Book Co., New York (1961).
6. D. H. Kaelble, "Peel Adhesion: Influence of Surface Energies and Adhesive Rheology", J. Adhesion, Vol. 1, (1969), p. 102.
7. A. V. Tobolsky, Properties and Structure of Polymers, Wiley, N. Y. (1962).
8. D. H. Kaelble, *Trans. Soc. Rheol., 4,* (1960), p. 45.
9. D. H. Kaelble, Ibid., 3, (1959), p. 161.